Journal of Applied Electrochemistry (2005) 35:1133–1139
DOI 10.1007/s10800-005-9001-2

Electrodeposition of Zn–Mn alloys in acidic and alkaline baths. Influence of additives on the morphological and structural properties

D. SYLLA, C. REBERE, M. GADOULEAU, C. SAVALL, J. CREUS and PH. REFAIT*
Laboratoire d'Etudes des Matériaux en Milieux Agressifs (LEMMA), EA3167, Université de La Rochelle, Bâtiment Marie Curie, Avenue Michel Crépeau, F-17042, La Rochelle Cedex 1, France
*(*author for correspondence, fax: + 33 5 46 45 72 72, e-mail: prefait@univ-lr.fr)*

Received 4 January 2005; accepted in revised form 22 June 2005

Key words: additives, cyclic voltammetry, electrodeposition, manganese, scanning electron microscopy, X-ray diffraction, Zn alloys

Abstract

Electrodeposition of Zn–Mn alloys on steel was achieved using alkaline pyrophosphate-based baths or acidic chloride-based baths. Cyclic voltammetry was used to determine the potential ranges where the various redox processes were taking place. It appeared that the reduction of Mn(II) was generally hidden by the other reduction reactions, especially by the hydrogen evolution reaction. Zn–Mn alloys containing up to 25 at.% Mn in the alkaline bath and 12 at.% in the acidic bath could be obtained at the cost of very low current efficiencies.The characterisation of the deposits obtained either by galvanostatic polarisation or potentiostatic polarisation was performed by Scanning Electron Microscopy and X-Ray Diffraction. Various Zn–Mn phases were obtained, depending on the current densities, the composition of the deposit and that of the electrolytic bath.Two commercial additives usually used for zinc electrodeposition, one in alkaline baths, the other in acidic baths, were tested. Their effects upon the composition, the morphology and the microstructure of the deposit were investigated.

1. Introduction

Electrodeposited coatings of zinc on mild steel sheet are widely used to provide corrosion protection. Since this protection is not acceptable under severe atmospheric conditions, various alternative methods and materials are being investigated. Various Zn-based alloys were considered, and for instance Zn–Ni, Zn–Co and Zn–Fe are currently used in industry. Several authors [1–4] have also investigated the Zn–Mn alloys. In a review article [5], Wilcox reports the results obtained by several corrosion studies, and concludes that the corrosion resistance in laboratory chloride environments is superior to zinc and other zinc alloys. The ability of Zn–Mn alloys (manganese content between 0 and 15%) to resist atmospheric corrosion was tested by Soto [6], who reports a significant improvement of their behaviour in a marine atmosphere in comparison with Zn or other Zn alloys. Several studies have shown that coatings only composed of the phase ε-ZnMn ensured the best protection ability [7, 8].

The components of the baths are commonly $ZnSO_4$ and $MnSO_4$ in Na-citrate as a necessary complexing agent to bring the deposition potentials closer, since the standard electrode potentials of the couples Zn^{2+}/Zn and Mn^{2+}/Mn in acidic medium are significantly different, −0.76 V/SHE for Zn vs −1.18 V/SHE for Mn. One of the problems of such baths is that the increase in Mn content is obtained with low current efficiency [2], and additives are used in order to improve the performance of the sulphate-citrate bath [9, 10]. Other electroplating solutions have been considered. On the one hand, the electrodeposition of Zn–Mn alloys from acidic chloride solutions in the absence of any complexing agent was achieved [11]. The electrolytic bath consisted in an acidic $ZnCl_2$, $MnCl_2$ and KCl solution buffered by H_3BO_3. On the other hand, Zn–Mn alloys were deposited at low current densities using ethylenediaminetetraacetic acid as the complexing agent for Zn(II) and malate or citrate as the complexing agent of Mn(II) [12].

Electrodeposition of Zn–Mn alloys using an alkaline bath has not been reported yet. Pyrophosphate, a complexing agent of both Zn(II) and Mn(II), was retained and solutions composed of $K_4(P_2O_7)$, $ZnSO_4{\cdot}7H_2O$ and $MnSO_4{\cdot}H_2O$ were tested. This work presents a comparison between the preliminary results obtained with an alkaline pyrophosphate-based bath and those obtained with the acidic $KCl + H_3BO_3$ bath. Deposits were synthesised with or without specific commercial additives

designed for zinc electrodeposition in acidic or alkaline media. Composition, structure and morphology of the Zn–Mn films were studied by SEM, EDS and XRD.

2. Experimental procedure

The electrochemical experiments were carried out in a classical three-electrode glass cell. The working electrode was a disk of 35 NCD16 steel disk (typical composition: 0.37% C, 3.8% Ni, 1.78% Cr, 0.41% Mn and 0.24% Si) with area of 0.78 cm^2. The steel surfaces were polished with silicon carbide (particle size 5 μm), sonicated for 2 min, rinsed thoroughly with Milli-Q water and dried. The reference electrode was a saturated calomel electrode (SCE) whereas the counter electrode was a zinc electrode. Cyclic voltammetry experiments were done at room temperature with a Perkin-Elmer EGG 273A potentiostat system.

The alkaline bath was composed of 1.0 mol l^{-1} $K_4P_2O_7$, 0.05 mol l^{-1} $ZnSO_4{\cdot}7H_2O$ and 0.05 mol l^{-1} $MnSO_4{\cdot}H_2O$. Pyrophosphate ions were used as complexing agents in order (i) to work in alkaline conditions without precipitating Mn and Zn hydroxides and (ii) to decrease the difference between zinc and manganese deposition potentials. The pH was adjusted at 9.5 by addition of H_2SO_4. Hydroxylamine (2 g l^{-1}) was used as a reducing agent to prevent oxidation of Mn(II) by dissolved oxygen. All the reagents were from Sigma-Aldrich with maximum purity.

The acidic bath was composed of 2.31 mol l^{-1} KCl, 0.4 mol l^{-1} H_3BO_3, 0.462 mol l^{-1} $ZnCl_2$ and 0.707 mol l^{-1} $MnCl_2$ [11]. The pH was adjusted at 4.9 by addition of KOH. Boric acid was reported to inhibit both hydrogen formation and zinc deposition [13] and to limit pH changes at the electrode surface during electrodeposition.

Zn–Mn codepositions were also realised using commercial additives commonly used for electrodeposition of zinc. The first one, devoted to alkaline baths, was added to the pyrophosphate-based electrolyte, the other, devoted to acidic baths, was added to the KCl + $ZnCl_2$ + $MnCl_2$ + H_3BO_3 electrolyte.

Scanning electron microscopy (SEM) was carried out on a JEOL 5410 Low Vacuum, and coupled microanalyses were performed using an energy dispersive X-ray spectrometer (EDS). ZAF corrections were applied to quantitative measurements. The crystal structures of the electrodeposited films were investigated by X-ray diffraction (XRD) on a Siemens apparatus using Cu-$K_{\alpha\ 1}$ radiation with $\lambda = 0.15406$ nm in a Bragg-Brentano geometry. The patterns were calibrated with the diffraction lines of the substrate (α-Fe).

3. Results and discussion

3.1. *Electrodeposition without additives*

The properties of the Zn-Mn electrodeposited films, that is the morphology determined by SEM and the nature of various Zn–Mn phases present, identified by XRD, are summarised in Table 1. They depend on the Mn content but differ significantly according to the electrolytic bath. For instance, the 12 at.% Mn deposit obtained in the acidic bath is composed of one single phase, ε-ZnMn, whereas the 15 at.% Mn deposit obtained in the alkaline bath, is composed of two phases, the ε phase and the η phase, that is Zn.

Cyclic voltammetry was performed previously in each electrolytic bath to determine the potential ranges where the electrochemical reactions were taking place. The voltammograms presented in Figure 1 were achieved at a scan rate of 20 mV s^{-1}, at room temperature, without stirring.

In the acidic bath (Figure 1a), Zn^{2+} reduction occurs at around −1.1 V/SCE, a value close to the theoretical deposition potential in this bath ($E_{eq} = -1.01$ V/SCE). The shape of the negative scan is characteristic of Zn^{2+} reduction with a broad current peak around −1.3 V/SCE followed by a large plateau. The cathodic current density increases drastically below −1.55 V/SCE which may correspond to hydrogen evolution and Mn^{2+} reduction. The deposition of manganese is then masked by the hydrogen evolution reaction. A series of potentiostatic experiments was performed and the deposits obtained at different deposition potentials (E_d) were analysed by SEM/EDS, allowing us to determine the threshold potential value corresponding to the incorporation of

Table 1. Deposits obtained without additives in an unstirred electrolyte at room temperature

Electrolyte	Current density j/mA cm^{-2};; and deposition potential E_d/V vs SCE	Mn content/at.%	Visual aspect of the deposit	Morphology	Phases obtained
Acid bath without additive	$j \sim -57$ mA cm^{-2}; $E_d = -1.5$ V	2.5	Grey, rough	Cauliflower	$\varepsilon+\zeta+\eta$(Zn)
	$j \sim -65$ mA cm^{-2}; $E_d = -1.55$ V	9	Grey, rough	Cauliflower	$\varepsilon+\zeta$
	$j \sim -140$ mA cm^{-2}; $E_d = -1.65$ V	12	Dark grey, rough	Cauliflower	ε
	$j < -150$ mA cm^{-2}		Black, burnt		
Alkaline bathwithout additive	$j \sim -40$ mA cm^{-2}; $E_d = -1.85$ V	4	Light grey, smooth	Nodules	$\varepsilon+\zeta+\eta$(Zn)
	$j \sim -70$ mA cm^{-2}; $E_d = -1.90$ V	15	Rough, non homogeneous, stripes	Nodules	$\varepsilon+\eta$(Zn)
	$j \sim -90$ mA cm^{-2}; $E_d = -1.95$ V	24	Rough, non homogeneous, stripes	Nodules	ε
	$j < -100$ mA cm^{-2}		Burnt		

manganese. We observed that for E_d between −1.1 V and −1.4 V/SCE, only zinc was deposited. In agreement with the voltammogram, Mn was deposited for E_d lower or equal to −1.5 V/SCE. At this potential value, the manganese content was about 2.5 at.%. This result confirms that Zn–Mn electrodeposition is normal [14].

The cathodic part of the anodic-going scan remains below the curve obtained during the cathodic-going scan. This is probably due to the formation of rough and dendritic deposits at very negative potentials. The active area, and thus the rate of hydrogen evolution, are increased. Looking to the anodic part of the positive scan, it can be seen that the dissolution potential is about −1.10 V/SCE, that is very close to the beginning of zinc deposition. Within the scan range, limited to −0.8 V/SCE in order to avoid the dissolution of the steel substrate, the anodic current increases continously.

The negative scan of the voltammogram obtained with the alkaline bath (Figure 1b) shows that the Zn^{2+} reduction begins at a lower potential, about −1.42 V/SCE, due to complexation with pyrophosphate. The peak at −1.45 V/SCE and the following large plateau correspond to the reduction of the Zn^{2+} complexes. As for the acidic bath, there is no characteristic peak related to Mn^{2+} reduction. Hydrogen evolution, responsible for the increase in the cathodic current below −1.8 V/SCE, masks the deposition of manganese. The difference between the negative and positive scans in the cathodic part of the voltammogram is quite small, which suggests that the deposit is less rough than that obtained in the acidic bath. On the anodic part of the positive scan, various oxidation peaks are visible between −1.4 and −1.0 V/SCE. These may be attributed to the dissolution of the different phases deposited at different potentials during the cathodic scan, e.g. zinc at high potentials and Zn–Mn phases at lower potentials. The experiments performed in potentiostatic mode confirm that potential values lower than −1.8 V/SCE must be applied in order to obtain Zn–Mn alloys. At −1.8 V/SCE, the manganese content is only 0.5 at.%.

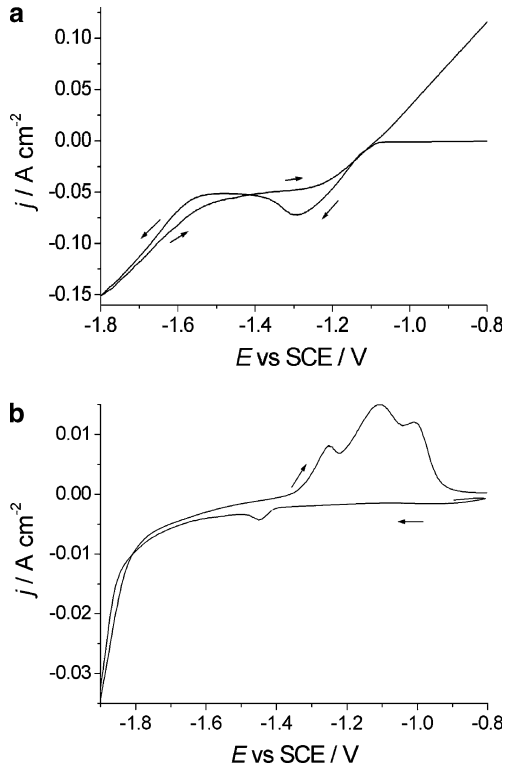

Fig. 1. Cyclic voltammograms for a 35NCD16 steel electrode (a) in the acidic chloride solution and (b) in the alkaline pyrophosphate-based solution. The electrolytes were not stirred and the scan rate was 20 mV s^{-1}.

The acidic bath produces deposits with a manganese content not exceeding 12 at.%. They are obtained at $E_d = -1.65$ V/SCE, with current densities around 140 mA cm^{-2}. The alkaline bath allows manganese contents up to 25 at.%. The SEM micrograph of the 12 at.% Mn deposit obtained in the unstirred acidic chloride solution (Figure 2a) is compared to that of the 15 at.% Mn deposit obtained at $E_d = -1.90$ V/SCE in the unstirred alkaline pyrophosphate solution (Figure 2b). The coating obtained in the acidic bath is rough, with a cauliflower-type morphology (maximum grain size of about 20 μm). This is due to the fact that large current densities have to be applied in order to obtain significant Mn contents in the coatings. The SEM micrograph of the coating obtained in the alkaline bath shows nodules with diameters smaller than 2 μm, that is a finer morphology than that observed in the acidic bath for a comparable composition. This results from the fact that pyrophosphate is a complexing agent. It adds a reaction step in the deposition process, modifies the electrocrystallisation and shifts the deposition potential towards lower values, favouring the nucleation and increasing the number of crystals thus decreasing their size. The EDS analyses revealed that the composition of the coatings obtained in the alkaline bath was not homogeneous: stripes, more likely due to the hydrogen release, are noticed. Moreover, above a thickness of a few micrometers these coatings do not adhere to the substrate. It can be suggested that after the deposition of the first micrometers, the interfacial pH, increased by the reduction of H_2O and the production of OH^- ions, becomes sufficient for the precipitation of zinc and/or manganese hydroxides. The presence of these hydroxides would then hinder the adherence of the Zn–Mn crystals.

For both baths, the growth tends to become dendritic for the highest manganese contents. In both cases, the hydrogen evolution reaction limits the manganese incorporation and, for the manganese richer deposits, leads to powdered coatings which can not be used as anti-corrosion coatings.

The corresponding XRD patterns are presented in Figure 3. The deposit obtained at −1.65 V/SCE in the acidic chloride bath is only composed of the HCP ε-ZnMn phase. According to the equilibrium diagram [15], the ε phase is thermodynamically stable only at T > 250 °C, between about 11 to 58 at.% Mn. The thermal stability of ε-ZnMn deposits has however been demonstrated [4]. The XRD pattern of the deposit obtained at −1.90 V/SCE in the alkaline phosphate bath

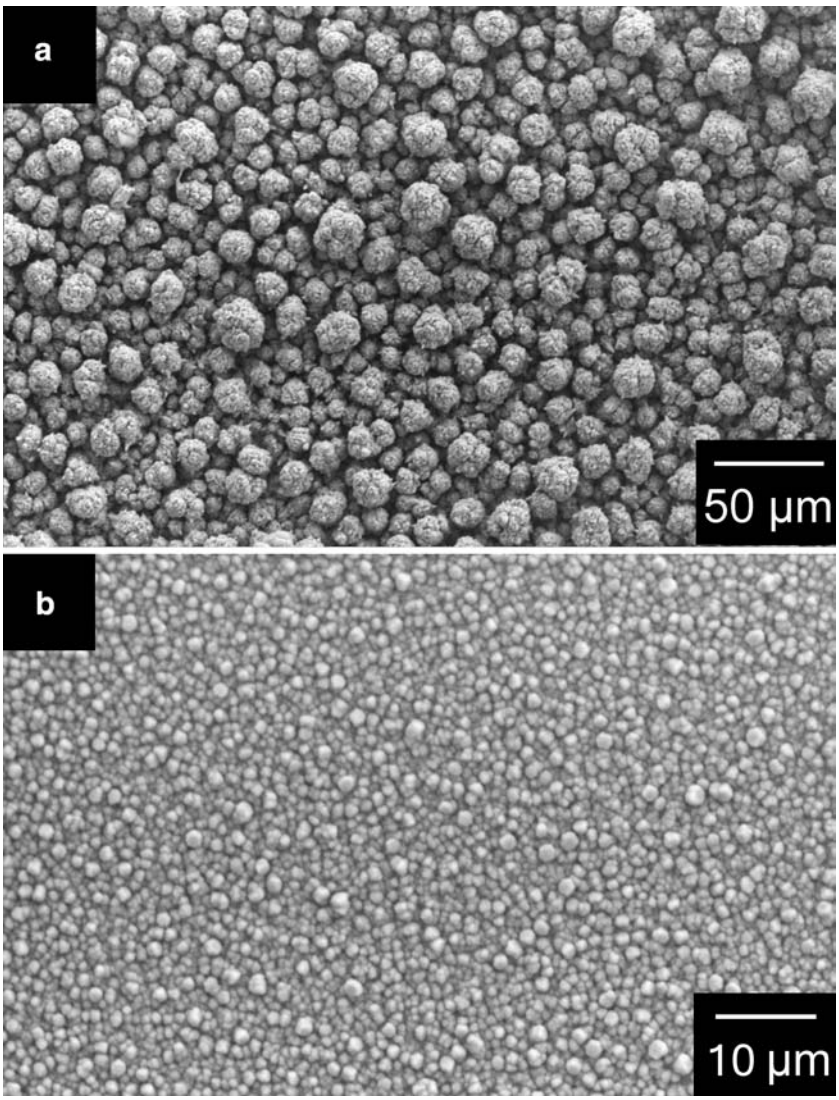

Fig. 2. SEM micrographs: (a) top view of the 12 at.% Mn deposit obtained at $E_d = -1.65$ V/SCE in the acidic chloride bath and (b) top view of the 15 at.% Mn deposit obtained at $E_d = -1.90$ V/SCE in the alkaline pyrophosphate-based bath. The electrolytes were not stirred.

is composed of the diffraction lines of the HCP phases ε-ZnMn and Zn (η). The Mn content, 15 at.%, is larger but, in this case, proves to be insufficient to lead to a monophasic ε-ZnMn deposit. Comparison with the previous XRD pattern clearly shows that the intensities of the ε diffraction lines have changed. The intensity of the 100 and 110 lines are abnormally small whereas the 002 line is abnormally intense. This indicates that the ε-ZnMn crystals are oriented preferentially with their basal plane parallel to the steel surface. Moreover, the 002 line is thinner, which indicates that the particles have grown essentially along the *c* direction, that is perpendicularly to the steel surface. It is possible that the presence of pyrophosphate in the alkaline bath hinder the growth of the ε phase crystals.

3.2. *Electrodeposition with commercial additives*

Different additives (polyethylene glycol, Triton X100, vanillin, commercial additives) were tested in order to improve the morphology of the deposits and facilitate Mn deposition. In this paper, the best results, obtained with commercial additives are presented.

The voltammograms are presented in Figure 4. In the acidic bath (Figure 4a), the negative scan begins with a large plateau where the current density is constant from −0.8 down to −1.5 V/SCE. This may be attributed to a strong blocking effect of the additive. Then, below −1.5 V/SCE, the cathodic current increases regularly as the potential decreases. The value of the current density, about −0.07 A cm^{-2} at −1.7 V/SCE, can be compared to that reached without the additive (Figure 1a), that is −0.12 A cm^{-2}. One of the effects of the additive is then to decrease the cathodic current at the more negative potentials where the hydrogen evolution occurs: it hinders clearly the reduction of protons. On the positive scan, the cathodic current density on the plateau still observed between −1.5 to −1.3 V/SCE is slightly larger than that measured on the negative scan. This phenomenon may have many origins. It may be a consequence

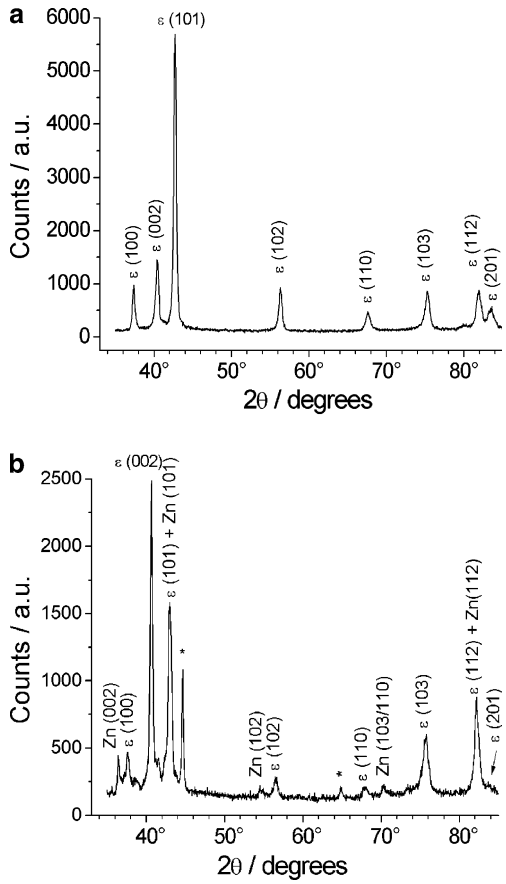

Fig. 3. XRD patterns of (a) the 12 at.% Mn deposit obtained at $E_d = -1.65$ V/SCE in the acidic chloride bath and (b) the 15 at.% Mn deposit obtained at $E_d = -1.90$ V/SCE in the alkaline pyrophosphate-based bath. The electrolytes were not stirred. * denotes the lines of the substrate, that is α-Fe.

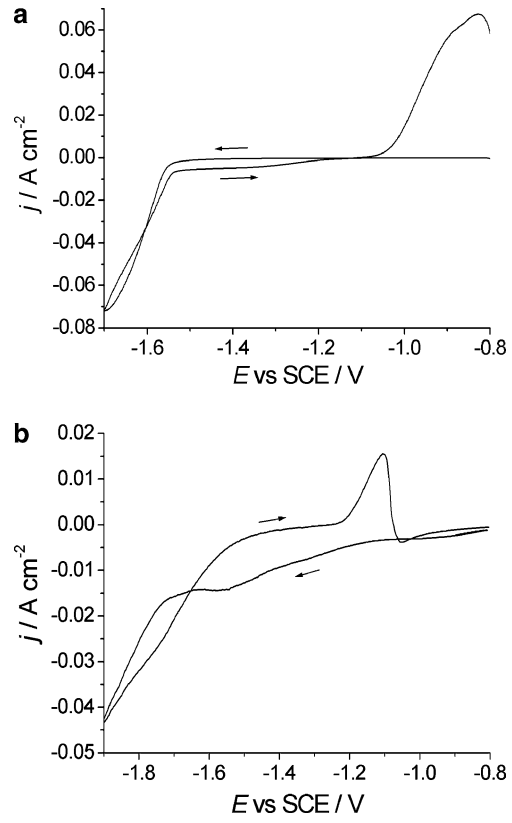

Fig. 4. Cyclic voltammograms for a 35NCD16 steel electrode (a) in the acidic chloride solution and (b) in the alkaline pyrophosphate-based solution, when commercial additives are used. The electrolytes were not stirred and the scan rate was 20 mV s^{-1}.

of an increase of the roughness of the electrode surface or it may result from the change in the chemical nature of the surface. During the negative scan, the substrate is steel, during the positive scan, the surface is coated with Zn–Mn alloy(s). The interactions of the additive with iron, zinc and manganese may be quite different. At about −1.3 V/SCE the current density begins to be more and more anodic, as the various phases deposited previously begin to dissolve.

In the alkaline bath (Figure 4b, that can be compared to Figure 1b), the commercial additive also modifies the shape of the voltammogram. First, the additive modifies strongly Zn(II) reduction. Without additive, this reaction is marked by a small peak at −1.45 V/SCE that reaches a maximum cathodic current density of -5×10^{-3} A cm^{-2}. With additive, the current density decreases regularly down to −0.015 A cm^{-2}, stabilises, and decreases again when water reduction is activated. In contrast, the reduction of water is scarcely affected. With or without additive, it begins to be active at the same potential, −1.75 V/SCE, and reaches similar current densities, −0.042 vs −0.034 A cm^{-2} at −1.9 V/SCE. On the positive scan, the only distinctive feature is the oxidation peak characteristic of the coating dissolution. It is less intense than the peak observed without additive. This may be due to the fact that the additive strongly reduces Zn(II) reduction and leads to a thinner coating. It could also result from partial inhibition of the coating dissolution by the additive.

A series of experiments in potentiostatic mode were performed as in section 3.1. They revealed that the additive used in the acidic bath facilitated the incorporation of manganese in the coating at lower current density. As an example, for the same deposition potential of −1.65 V/SCE, the manganese deposit content increased from 12% (without additive) to about 22% (with additive). At the same time, the current density varied from −140 to −115 mA cm^{-2}. In contrast, with the additive used in the alkaline bath, a larger current density was required to deposit Zn–Mn alloy coatings. For instance, a manganese content of about 24% was obtained with this additive, at the cost of a strong increase of the cathodic current, that is −230 mA cm^{-2} instead of −90 mA cm^{-2} without additive. Consequently, it is clear that this addititive does not shift only Zn(II) reduction towards more negative potentials, but also Mn(II) reduction.

SEM was used in order to precise the morphology of the deposits obtained with the additives (Figure 5). The additive used with the acidic bath leads to smoother and more compact deposits (Figure 5a, that could be compared to Figure 2a). Moreover, the morphology of the coatings is drastically modified. It is no longer a

cauliflower morphology, that is a more or less dendritic growth, even for the highest manganese contents or the thickest deposits. The deposit is made of an assembly of pyramidal crystals with maximum size of ~ 2 μm. This morphology is observed for manganese contents between 6 and 22%. A morphology showing hexagonal pyramids very similar to Figure 5a was reported by Bozzini et al. [10], in a sulphate-citrate bath in the presence of thiocarbamide. They attributed the change of morphology induced by the additive to the adsorption of organic agents. They also noted that the morphology of Zn–Mn generally evolved from platelets (for the lower manganese contents), to globules as the current density increased. Muller et al. [12], by adding EDTA or other complexing agents, reported various morphologies (platelets, nodules, polyhedral grains or rounded grains of different sizes), whereas the major phase detected by XRD was the ε phase, sometimes mixed with γ-ZnMn or pure zinc.

The additive used with the alkaline bath also leads to smooth, semibright and adherent coatings. The thickness can be increased up to at least 20 μm. The composition was investigated by EDS along a cross section of the deposit (not represented) and proves to be homogenous. The SEM micrograph of Figure 5b shows the typical morphology induced by the additive. The surface is very smooth, and the deposit appears as an almost uniform layer without well-defined geometric characteristics. Only a few small nodules, slightly emerging from the nearly uniform layer, can be seen. This suggests that the deposit is mainly made of very small crystals that cannot be distinguished at that scale. In conclusion, the additives improved the morphology of the deposits in both baths.

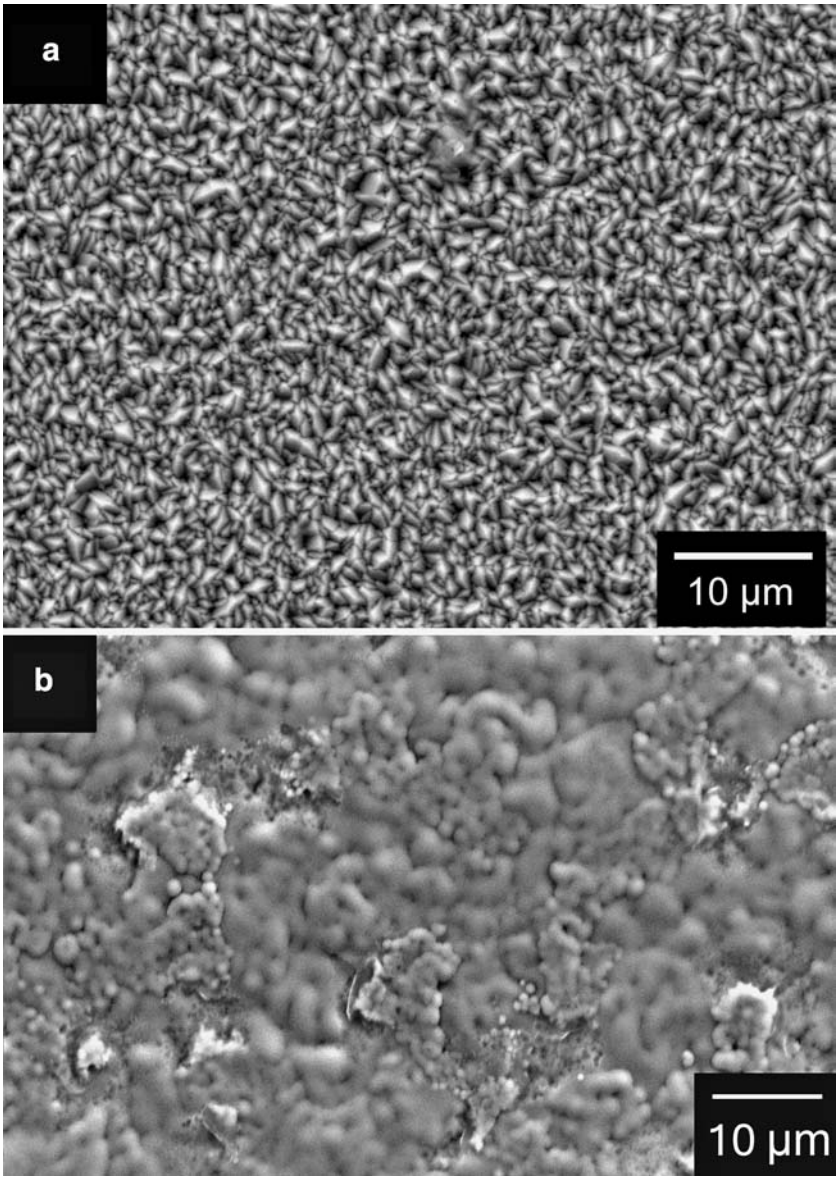

Fig. 5. SEM micrographs: (a) top view of the 22 at.% Mn deposit obtained at $E_d = -1.65$ V/SCE in the acidic chloride bath and (b) top view of the 24 at.% Mn deposit obtained at $E_d = -2.50$ V/SCE in the alkaline pyrophosphate-based bath, when commercial additives are used.

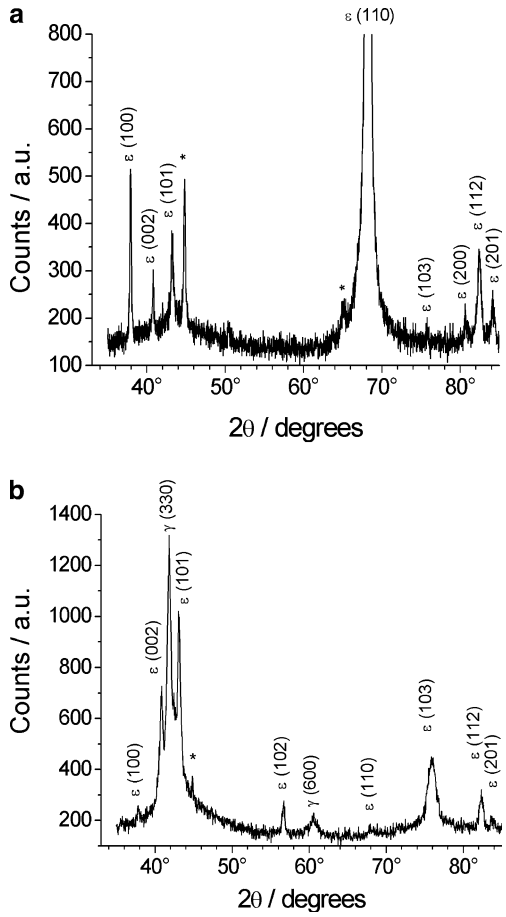

Fig. 6. XRD patterns of (a) the 22 at.% Mn deposit obtained at $E_d = -1.65$ V/SCE in the acidic chloride bath and (b) the 24 at.% Mn deposit obtained at $E_d = -1.90$ V/SCE in the alkaline pyrophosphate-based bath, when commercial additives are used. The electrolytes were not stirred. * denotes the lines of the substrate, that is α-Fe.

XRD patterns are displayed in Figure 6. The deposit formed in the acidic chloride bath is still monophasic, containing only the HCP ε Zn–Mn phase. The main effect of the additive was to hinder the crystal growth in certain directions, constraining the ε phase particles to develop with their basal plane perpendicular to the steel surface. This is demonstrated by the intensity of the 110 line. Actually, the intensity scale of the pattern was restricted to 2% of the 110 line intensity.

The ε phase is still present in the Zn–Mn films electrodeposited with the alkaline pyrophosphate bath, but it is now obtained together with the γ-phase. γ-ZnMn is the stable phase at room temperature for Mn contents around 20 at.% [15]. It is characterised by a γ-brass structure.

4. Conclusion

Morphology and crystal structure of the deposits depend on the electrolytic bath. In the absence of additives, for the same Mn content, the alkaline bath leads to a smaller grain size, typically 1–3 μm instead of 10–25 μm. At 15 at.% Mn, the deposit still contains Zn particles, whereas, for the acid bath, it is monophasic, made of the HCP ε-ZnMn phase, even for a lower Mn content of 12 at.%.

Commercial additives were used in order to facilitate manganese incorporation, to limit hydrogen evolution reaction, and to prevent the dendritic growth that leads to porous deposits. In each case, the additive improves the visual appearance of the coatings and leads to adherent and compact layers with more than 20 at.% of manganese. However, the additive chosen for the alkaline bath inhibits both zinc and manganese deposition and it becomes necessary to shift the deposition potential negatively in order to incorporate manganese. Moreover, this additive promotes hydrogen evolution. The 24 at.% Mn deposit obtained in the alkaline bath is composed of two phases, the metastable ε phase and the stable γ phase.

In contrast, the additive used with the acidic bath inhibits only the zinc deposition significantly. Thus, the additive increases the manganese content of the deposit which varies for instance from 12 to 22% at $E_d = -1.65$ V/SCE. It also induces a drastic change in morphology, leading to a pyramidal-type morphology instead of the cauliflower-type morphology observed without additive. The 22 at.% Mn deposit is still monophasic.

References

1. G. Govindarajan, V. Ramakrishnan, S. Ramamurthi, V. Subramanian and N.V. Parthasaradhy, *Bull. Electrochem.* **5** (1989) 422.
2. M. Eyraud, A. Garnier, F. Mazeron and J. Crousier, *Plat. Surf. Finish.* **82** (1995) 63.
3. B. Bozzini, G. Bollini, P.L. Cavalloti and F. Pavan. "Electrodeposition of Zn-Mn alloys on steel" (text in italian). Proc. 25° Convegno Nazionale AIM (National congress of the Italian Metallurgical Society), 12–14 Oct. 1994, Milano Vol. 2, p.122.
4. B. Bozzini, F. Pavan, G. Bollini and P.L. Cavallotti, *Trans. Inst. Met. Finish.* **75** (1997) 175.
5. G.D. Wilcox and B. Petersen, *Trans. Inst. Met. Finish.* **74** (1996) 115.
6. F. Sotto, Ph.D. Thesis, Université de Provence – Aix Marseille 1 (1998).
7. T. Andreu, Ph.D. Thesis, Universitat de Barcelona, Departament De Química Física (2004).
8. M. Sagiyama, T. Urakawa, T. Adaniya and T. Hara, SAE (1986) Technical paper n° 860268, 107.
9. B. Bozzini, E. Griskonis, A. Sulcius and P.L. Cavallotti, *Plat. Surf. Finish.* **88** (2001) 64.
10. B. Bozzini, E. Griskonis, A. Fanigliulo and A. Sulcius, *Surf. Coat. Technol.* **154** (2002) 294.
11. D. Sylla, J. Creus, C. Savall, O. Roggy, M. Gadouleau and Ph. Refait, *Thin Solid Films* **424/2** (2003) 171.
12. C. Müller, M. Sarret and T. Andreu, *J. Electrochem. Soc.* **149** (2002) C600.
13. C. Karwas and T. Hepel, *J. Electrochem. Soc.* **135** (1988) 839.
14. A. Brenner, *Electrodeposition of Alloys* Vol. II (Academic Press, New york, 1963), pp. 152.
15. P.M. Hansen, *Constitution of Binary Alloys*, 2nd ed., (Mc Graw-Hill Book Co, New York, NY, 1958), pp. 962–963.